DELFT UNIVERSITY OF TECHNOLOGY

REPORT 95-131

Higher order flux-limiting methods for steady-state, multidimensional, convection-dominated flow

M. Zijlema and P. Wesseling

ISSN 0922-5641

Reports of the Faculty of Technical Mathematics and Informatics no. 95-131

Delft 1995

Abstract

Numerical modeling of convection suitable for finite volume methods for steady-state, multidimensional, incompressible, turbulent flows is considered. Two methods used to achieve higher order accurate and oscillation-free solutions are discussed, namely flux limiting and variable normalization. A unified formulation, which brings together most existing higher order monotonicity preserving schemes, is discussed. The unified formulation allows the inclusion of higher order non-monotone schemes, and a new class of flux limiters is presented. Some numerical results are shown for two-dimensional flows, and the superiority of the flux-limiting schemes is confirmed by comparison with results of the first order upwind scheme.

1 Introduction

The last decade has seen a considerable increase in computer capacity with regard to speed and memory. With this background, a large number of numerical algorithms based on a finite volume formulation of the Navier-Stokes equations in boundary-fitted coordinates with turbulence modeling has been developed for the computation of steady-state incompressible turbulent flow in complicated domains [4, 22, 17, 3, 15, 40]. Most of the numerical procedures are based on second order central differencing for the spatial derivatives. In many practical problems the Reynolds number is high, and it is well known that in these circumstances central differences may give rise to non-physical spatial oscillations. In addition, they are unsuitable for two-equation turbulence models, for instance the k-ε variant [12], for these cannot accept (unphysically) negative values of turbulence quantities arising as a result of oscillations, and instability will occur due to their nonlinear nature. To overcome these problems the hybrid central/upwind scheme of [25] and other first order variants, such as PLDS [21], are frequently invoked. These schemes are popular because of their robustness, but they suffer from severe numerical diffusion when the grid is not fine enough or when the flow direction is not aligned with the local grid direction.

Higher order schemes which avoid the unfavorable properties mentioned above, can be regarded as best suited for general flow computations. However, the monotonicity constraint to first order schemes has to be replaced by a less restrictive total variation diminishing (TVD) requirement [8]. Also, such schemes should be algorithmically simple, because only simple schemes can find widespread use in practical engineering calculations.

The present paper aims to draw together two methods of formulating higher order schemes, which produce oscillation-free solutions and minimize numerical diffusion. One method that we discuss is the construction of flux limiters to obtain TVD schemes, described in [28]. Traditionally, such schemes have been designed for the unsteady compressible Euler equations.

Moreover, the TVD condition has been proved completely for the one-dimensional case. The issue given attention here is the extension of this work to the steady-state, multidimensional transport equations for incompressible turbulent flows. Upwind-weighted as well as symmetric flux limiters have been proposed in the literature and will be presented in this paper. The first group of limiters includes Van Leer [30], Chakravarthy-Osher discussed in [28], the limited $\kappa = \frac{1}{3}$-scheme proposed by Koren [11] and ISNAS presented in [39], the latter enclosing Van Leer's MUSCL [31] and UMIST [16]. The second method is the normalized variable (NV) technique based on [14] and [6]. It is suitable for steady-state calculations. A number of proposed NV schemes, such as SMART [6], HLPA [37], SOUCUP [38] and BSOU [20], will be considered. In general, flux-limiting algorithms are more convenient than NV methods, since a defect correction approach can easily be adopted.

In what follows, the non-monotone, the flux-limiting and the NV schemes for a one-dimensional convection equation, and their extensions to the two-dimensional case are outlined. A unified formulation of these developments is discussed. Then, five classes of flux limiters are presented, which bring together all flux-limiting and NV schemes mentioned. One of these classes is proposed in this paper. Finally, we show some numerical results in which the performance of a number of flux-limiting schemes are examined by means of a comparison of numerical accuracy and computational cost. The comparison is made on the basis of applications to two test problems, both involving convection dominance. Also, the application of one of the flux-limiting schemes, namely ISNAS, to turbulent flow is demonstrated.

2 Higher order schemes and monotonicity

In [40] the finite volume discretization of the steady-state, incompressible Navier-Stokes and turbulence transport equations in general coordinates on a staggered grid is discussed. The accuracy with which convective transport, in particular for turbulence quantities, is approximated is of crucial importance and is the subject of this paper.

Let us consider the following one-dimensional scalar convection equation:

$$\frac{\partial \phi}{\partial t} + \frac{\partial u\phi}{\partial x} = 0 \tag{2.1}$$

where ϕ is a scalar quantity being convected by a velocity u. A uniform infinite staggered grid is given in Figure 2.1. Spatial discretization of (2.1) is obtained by integration over a

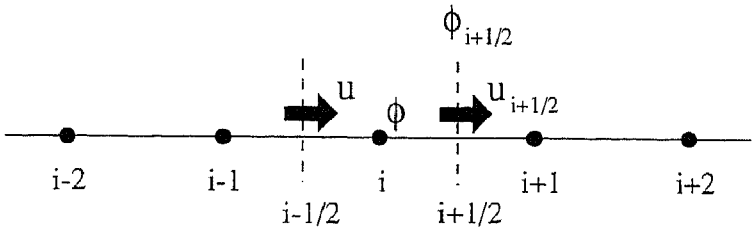

Figure 2.1: One-dimensional staggered grid showing the nodes involved in the evaluation of ϕ at cell-face $i + \frac{1}{2}$.

finite volume $\Omega_i = (x_{i-1/2}, x_{i+1/2})$:

$$\frac{\partial \phi}{\partial t} = -\frac{u_{i+1/2}\phi_{i+1/2} - u_{i-1/2}\phi_{i-1/2}}{\Delta x} \tag{2.2}$$

where Δx is the mesh-width. Throughout the paper the implicit Euler scheme is used in which the semi-discrete equation (2.2) is solved one time-step after another, using the time history merely as a route to steady-state. We discuss several methods for expressing the cell-face values $\phi_{i-1/2}$ and $\phi_{i+1/2}$ in terms of surrounding nodal values. We need to consider only the cell-face value $\phi_{i+1/2}$. The other face value will be treated in the same way. Furthermore, we assume that $u_{i+1/2} > 0$.

Approximations of the cell-face values can be constructed by piecewise polynomial interpolation as suggested in [32]. The basic idea of this so-called κ-interpolation is that linear and quadratic approximations of the solution on each cell lead to second- and third order space discretizations, respectively. The general form of the κ-scheme is

$$\phi_{i+1/2} = \phi_i + \frac{1}{4}[(1+\kappa)(\phi_{i+1} - \phi_i) + (1-\kappa)(\phi_i - \phi_{i-1})] \tag{2.3}$$

where the parameter $\kappa \in [-1, 1]$ is still to be chosen. Examples are the second order Fromm's scheme [5], the second order QUICK scheme proposed by Leonard [13] and the third order cubic interpolation scheme (CUI) used in [2] and are obtained by setting $\kappa = 0, \frac{1}{2}$ and $\frac{1}{3}$, respectively. For $\kappa \neq \frac{1}{3}$ the local truncation error is of second order; for $\kappa = \frac{1}{3}$ it is of third order.

Although higher order schemes have been successful in eliminating numerical diffusion, they may cause spurious oscillations in regions where large gradients exist. In the next two sections we discuss two methods to design higher order schemes which do not exhibit wiggles.

2.1 Flux-limiting technique

In [8] the total variation diminishing (TVD) concept is proposed as the criterion for developing convection schemes which combine accuracy and monotonicity. We study the following subset of implicit schemes applied to (2.1):

$$\phi_i^{n+1} = \phi_i^n - C_{i-1/2}^{n+1}(\phi_i^{n+1} - \phi_{i-1}^{n+1}) + D_{i+1/2}^{n+1}(\phi_{i+1}^{n+1} - \phi_i^{n+1}) \tag{2.4}$$

with

$$C_{i-1/2}^{n+1} = C(\phi_{i-2}^{n+1}, \phi_{i-1}^{n+1}, \phi_i^{n+1}, \phi_{i+1}^{n+1}), \quad D_{i+1/2}^{n+1} = D(\phi_{i-1}^{n+1}, \phi_i^{n+1}, \phi_{i+1}^{n+1}, \phi_{i+2}^{n+1}) \tag{2.5}$$

where n is a time level. The total variation of a numerical solution $\{\phi_i\}$ is defined by

$$\mathrm{TV}(\phi) = \sum_i |\phi_{i+1} - \phi_i| \tag{2.6}$$

and the scheme (2.4) is said to be TVD if

$$\mathrm{TV}(\phi^{n+1}) \leq \mathrm{TV}(\phi^n) \tag{2.7}$$

A grid function $\{\phi_i\}$ is called monotone if for all i

$$\min(\phi_{i-1}, \phi_{i+1}) \leq \phi_i \leq \max(\phi_{i-1}, \phi_{i+1}) \tag{2.8}$$

The scheme (2.4) is called monotonicity preserving if ϕ^{n+1} remains monotone when ϕ^n is monotone. Hence, no new minima or maxima are created during time advancement. In [8] it is shown that a nonlinear TVD scheme is monotonicity preserving. In [8] a class of explicit schemes is considered and conditions are derived to ensure that these schemes are TVD. For the implicit scheme (2.4) we have the following theorem.

Theorem 2.1 *If*

$$C_{i+1/2}^{n+1} \geq 0, \quad D_{i+1/2}^{n+1} \geq 0 \tag{2.9}$$

then scheme (2.4) is TVD.

Proof Subtracting equations (2.4) at $i+1$ and at i gives

$$\begin{aligned} \phi_{i+1}^n - \phi_i^n &= (1 + C_{i+1/2}^{n+1} + D_{i+1/2}^{n+1})(\phi_{i+1}^{n+1} - \phi_i^{n+1}) \\ &\quad -C_{i-1/2}^{n+1}(\phi_i^{n+1} - \phi_{i-1}^{n+1}) - D_{i+3/2}^{n+1}(\phi_{i+2}^{n+1} - \phi_{i+1}^{n+1}) \end{aligned} \tag{2.10}$$

Since (2.9) holds, we have

$$\begin{aligned} |\phi_{i+1}^n - \phi_i^n| &\geq (1 + C_{i+1/2}^{n+1} + D_{i+1/2}^{n+1})|\phi_{i+1}^{n+1} - \phi_i^{n+1}| \\ &\quad -C_{i-1/2}^{n+1}|\phi_i^{n+1} - \phi_{i-1}^{n+1}| - D_{i+3/2}^{n+1}|\phi_{i+2}^{n+1} - \phi_{i+1}^{n+1}| \end{aligned} \tag{2.11}$$

so that, using the fact that the grid is infinite,

$$\begin{aligned} TV(\phi^n) &= \sum_i |\phi_{i+1}^n - \phi_i^n| \\ &\geq \sum_i (1 + C_{i+1/2}^{n+1} + D_{i+1/2}^{n+1})|\phi_{i+1}^{n+1} - \phi_i^{n+1}| - \sum_i C_{i+1/2}^{n+1}|\phi_{i+1}^{n+1} - \phi_i^{n+1}| \\ &\quad - \sum_i D_{i+1/2}^{n+1}|\phi_{i+1}^{n+1} - \phi_i^{n+1}| = \sum_i |\phi_{i+1}^{n+1} - \phi_i^{n+1}| = TV(\phi^{n+1}) \end{aligned} \tag{2.12}$$

■

The construction of nonlinear TVD schemes is based on the flux-limiting formulation as presented in [28]. We write the face value $\phi_{i+1/2}$ as the sum of a diffusive first order upwind term and an "anti-diffusive" one. The higher order anti-diffusive part is multiplied by the so-called flux limiter, which is a nonlinear function of

$$r_{i+1/2} = \frac{\phi_{i+1} - \phi_i}{\phi_i - \phi_{i-1}} \tag{2.13}$$

leading to the flux-limited scheme

$$\phi_{i+1/2} = \phi_i + \frac{1}{2}\Psi(r_{i+1/2})(\phi_i - \phi_{i-1}) \tag{2.14}$$

Note that (2.13) is the inverse of the definition used in [28]. A scheme (2.14) is symmetric if the forward and backward gradients can be exchanged, so that the scheme can also be written as

$$\phi_{i+1/2} = \phi_i + \frac{1}{2}\Psi(\frac{1}{r_{i+1/2}})(\phi_{i+1} - \phi_i) \tag{2.15}$$

From (2.14) and (2.15) it follows that a symmetric limiter satisfies

$$\Psi(r) = r\Psi(\frac{1}{r}) \tag{2.16}$$

The flux limiter $\Psi(r)$ must satisfy certain constraints in order to satisfy the TVD condition (2.9). For example, with constant $u > 0$ substitution of (2.14) in (2.2) gives, using implicit Euler time discretization,

$$\begin{aligned} \phi_i^{n+1} &= \phi_i^n - \frac{u\Delta t}{\Delta x}(\phi_{i+1/2}^{n+1} - \phi_{i-1/2}^{n+1}) \\ &= \phi_i^n - \frac{u\Delta t}{\Delta x}[1 + \frac{1}{2}\Psi(r_{i+1/2}) - \frac{1}{2}\frac{\Psi(r_{i-1/2})}{r_{i-1/2}}](\phi_i^{n+1} - \phi_{i-1}^{n+1}) \end{aligned} \tag{2.17}$$

where Δt is the time-step. According to Theorem 2.1, the scheme is TVD if

$$1 + \frac{1}{2}\Psi(r) - \frac{1}{2}\frac{\Psi(s)}{s} \geq 0, \quad \forall r,\ s \tag{2.18}$$

This inequality is satisfied if

$$0 \leq \Psi(r) \leq 2r \tag{2.19}$$

Among the proposals, which have been discussed in, for example, [28] and [1], the following limiters are commonly used:

$$\begin{aligned} &\Psi(r) = (r + |r|)/(1 + r) && \text{Van Leer limiter} \\ &\Psi_\psi(r) = \max[\,0, \min(r, \psi)\,] && \text{Chakravarthy-Osher limiter} \\ &\Psi_\Phi(r) = \max[\,0, \min(\Phi r, 1), \min(r, \Phi)\,] && \text{Sweby } \Phi\text{-limiter} \end{aligned} \tag{2.20}$$

where $1 \leq \psi \leq 2$ and $1 \leq \Phi \leq 2$. The parameters ψ and Φ generate a family of limiters. For example, $\psi = 1$ or $\Phi = 1$ gives the well-known Minmod limiter which is the most diffusive one, and $\Phi = 2$ corresponds to a limiter which has been known in the literature as Roe's Superbee limiter and is less diffusive than Van Leer and Minmod. With the exception of the Chakravarthy-Osher limiter ($\psi \neq 1$), all these limiters share the symmetry property (2.16).

It is widely accepted that all TVD schemes must reduce locally to first order accuracy at physical extrema regardless of the order of accuracy in regions of monotonicity, so that $\Psi(r) = 0$ when $r \leq 0$ (see e.g. [28]), but this is a misunderstanding. It is shown here that TVD schemes need not be first order accurate at extrema of the solution, if the flux limiters are appropriately designed. We consider a semi-discrete TVD scheme (2.2) with constant $u > 0$ with the flux $\phi_{i+1/2}$ given by (2.14).

Theorem 2.2 *The necessary and sufficient condition for scheme (2.2), (2.14) to be second order accurate away from extrema of the solution is*

$$\Psi(1) = 1 \tag{2.21}$$

and second order accurate at extrema is

$$3\Psi(\frac{1}{3}) - \Psi(-1) = 2 \tag{2.22}$$

Proof Using the Taylor series we obtain

$$\begin{aligned} \frac{\phi_{i+1/2} - \phi_{i-1/2}}{\Delta x} &= (1 + \frac{1}{2}\Psi(r_{i+1/2}) - \frac{1}{2}\Psi(r_{i-1/2}))\phi_i' - \\ &\quad (\frac{1}{2} + \frac{1}{4}\Psi(r_{i+1/2}) - \frac{3}{4}\Psi(r_{i-1/2}))\Delta x\phi_i'' + \mathcal{O}(\Delta x^2) \end{aligned} \tag{2.23}$$

Taylor expansions of $r_{i+1/2}$ and $r_{i-1/2}$ about point x_i away from extrema (i.e. $\phi_i' \neq 0$) are given by

$$r_{i+1/2} = 1 + \mathcal{O}(\Delta x), \quad r_{i-1/2} = 1 + \mathcal{O}(\Delta x) \tag{2.24}$$

Obviously, $\Psi(1) = 1$ is the necessary and sufficient condition for (2.23) to be second order accurate. If x_i is an extremum, then $\phi_i' = 0$ but, in general, $\phi_i'' \neq 0$, so the condition for (2.23) to be second order accurate is

$$\frac{1}{2} + \frac{1}{4}\Psi(r_{i+1/2}) - \frac{3}{4}\Psi(r_{i-1/2}) = 0 \tag{2.25}$$

Furthermore, if $\phi_i' = 0$ then

$$r_{i+1/2} = -1 + \mathcal{O}(\Delta x), \quad r_{i-1/2} = \frac{1}{3} + \mathcal{O}(\Delta x) \tag{2.26}$$

Substitution in (2.25) gives (2.22).

■

This theorem suggests that one may allow $\Psi(r) \neq 0$ for $r \leq 0$ and Ψ may also be negative. A less restrictive sufficient condition than (2.19) for the implicit scheme (2.17) to be TVD is

$$\alpha \leq \Psi(r), \quad \frac{\Psi(r)}{r} \leq 2 + \alpha, \quad -2 \leq \alpha \leq 0 \tag{2.27}$$

It is easily seen that (2.18) is satisfied. Condition (2.19) is obtained as the special case $\alpha = 0$, so that (2.27) is more general. This idea is not new; see [27]. Figure 2.2 shows the set of values

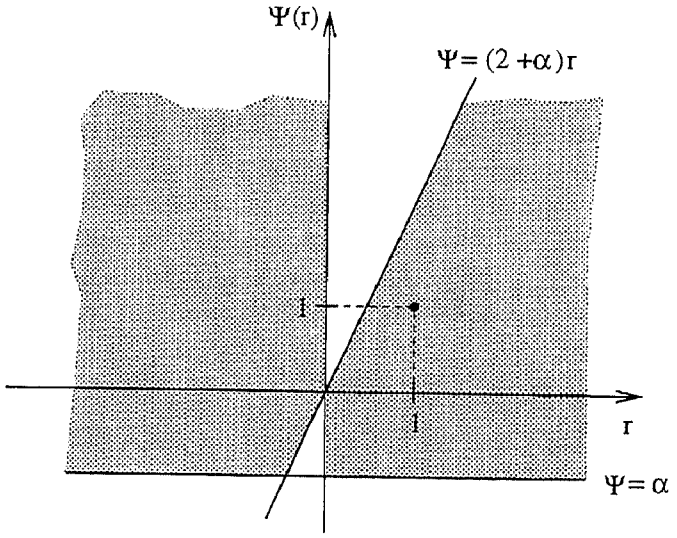

Figure 2.2: Region of limiters for implicit TVD schemes.

$\Psi(r)$ (shaded) satisfying (2.27). Condition (2.27) offers the possibility to construct limiters which are continuously differentiable everywhere, resulting in robust convergence of iterative solution methods. Examples of such limiters are the well-known Van Albada limiter discussed in [26], [27] and the recently proposed OSPRE limiter [35] which are given by, respectively:

$$\Psi(r) = \frac{r^2 + r}{r^2 + 1}, \quad \Psi(r) = \frac{3}{2}\frac{r^2 + r}{r^2 + r + 1} \tag{2.28}$$

These limiters satisfy (2.27) with $\alpha = -0.25$ and $\alpha = -0.5$, respectively. They do not satisfy (2.22), so the scheme (2.2) becomes diffusive at extrema (but less than the first order upwind scheme).

The situation is more unfavorable for multidimensional flow problems, since in [7] it is shown that any conservative TVD scheme in two space dimensions for scalar conservation laws is at most first order accurate. However, numerical experiments have shown that 2D schemes using an 1D second order accurate TVD scheme in each direction perpendicular to the cell face give oscillation-free accurate results. This has been understood since the introduction

of a new monotonicity concept weaker than TVD in two space dimensions in [26, 27]. We consider the following 2D scalar convection equation:

$$\frac{\partial \phi}{\partial t} + \frac{\partial u\phi}{\partial x} + \frac{\partial v\phi}{\partial y} = 0 \tag{2.29}$$

discretized by

$$\begin{aligned} \phi_{i,j}^{n+1} &= \phi_{i,j}^{n} - A_{i-1/2,j}^{n+1}(\phi_{i,j}^{n+1} - \phi_{i-1,j}^{n+1}) + B_{i+1/2,j}^{n+1}(\phi_{i+1,j}^{n+1} - \phi_{i,j}^{n+1}) \\ &\quad -C_{i,j-1/2}^{n+1}(\phi_{i,j}^{n+1} - \phi_{i,j-1}^{n+1}) + D_{i,j+1/2}^{n+1}(\phi_{i,j+1}^{n+1} - \phi_{i,j}^{n+1}) \end{aligned} \tag{2.30}$$

where

$$\begin{aligned} A_{i-1/2,j}^{n+1} &= A(\phi_{i-2,j}^{n+1}, \phi_{i-1,j}^{n+1}, \phi_{i,j}^{n+1}, \phi_{i+1,j}^{n+1}) \\ B_{i+1/2,j}^{n+1} &= B(\phi_{i-1,j}^{n+1}, \phi_{i,j}^{n+1}, \phi_{i+1,j}^{n+1}, \phi_{i+2,j}^{n+1}) \\ C_{i,j-1/2}^{n+1} &= C(\phi_{i,j-2}^{n+1}, \phi_{i,j-1}^{n+1}, \phi_{i,j}^{n+1}, \phi_{i,j+1}^{n+1}) \\ D_{i,j+1/2}^{n+1} &= D(\phi_{i,j-1}^{n+1}, \phi_{i,j}^{n+1}, \phi_{i,j+1}^{n+1}, \phi_{i,j+2}^{n+1}) \end{aligned} \tag{2.31}$$

In [26, 27], a class of explicit schemes in two dimensions is considered and a new definition of monotonicity is introduced which is weaker than TVD. Extending this to the implicit case, we have

Definition 2.1 *Scheme (2.30) is called monotone if*

$$A_{i-1/2,j}^{n+1} \geq 0, \quad B_{i+1/2,j}^{n+1} \geq 0, \quad C_{i,j-1/2}^{n+1} \geq 0, \quad D_{i,j+1/2}^{n+1} \geq 0 \tag{2.32}$$

According to Theorem 2.1, a 1D monotone implicit scheme is TVD and vice versa. In two dimensions, the total variation of $\{\phi_{i,j}\}$ is defined by (see [7])

$$\mathrm{TV}(\phi) = \sum_{i,j}(|\phi_{i+1,j} - \phi_{i,j}| + |\phi_{i,j+1} - \phi_{i,j}|) \tag{2.33}$$

Spekreijse shows that for explicit schemes, a 2D monotone scheme is not necessarily TVD [27]. This is also true for implicit schemes. For example, let $\{\phi_{i,j}^{n}\}$ be given by

$$\phi_{i,j}^{n} = \begin{cases} 1, & (i,j) = (1,0) \\ 0, & \forall (i,j) \neq (1,0) \end{cases}$$

and let in (2.30)

$$\begin{aligned} &A_{i-1/2,j}^{n+1} = B_{i+1/2,j}^{n+1} = C_{i,j-1/2}^{n+1} = D_{i,j+1/2}^{n+1} = 0, \quad \forall (i,j) \neq (0,0) \\ &B_{1/2,0}^{n+1} = 1, \quad A_{-1/2,0}^{n+1} = C_{0,-1/2}^{n+1} = D_{0,1/2}^{n+1} = 0 \end{aligned}$$

Then

$$\phi_{i,j}^{n+1} = \begin{cases} 1, & (i,j) = (1,0) \\ \frac{1}{2}, & (i,j) = (0,0) \\ 0, & \text{otherwise} \end{cases}$$

Hence, $\mathrm{TV}(\phi^n) = 4$ and $\mathrm{TV}(\phi^{n+1}) = 5$, so we found a monotone scheme which is not TVD.

The advantage of schemes satisfying (2.32) is brought out in the following theorem.

Theorem 2.3 (cf. [26, 27]). *If scheme (2.30) is monotone then a steady state solution of (2.30) is monotone, i.e., for all (i,j)*

$$\min(\phi_{i-1,j}, \phi_{i+1,j}, \phi_{i,j-1}, \phi_{i,j+1}) \leq \phi_{i,j} \leq \max(\phi_{i-1,j}, \phi_{i+1,j}, \phi_{i,j-1}, \phi_{i,j+1}) \tag{2.34}$$

where $\{\phi_{i,j}\}$ *denotes a steady-state solution of (2.30).*

For reasons of robustness and algorithmic simplicity, multidimensional flux-limiting schemes are treated by one-dimensional decomposition in the normal direction for each cell face. When applied to (2.29) with constants $u, v > 0$, the implicit Euler scheme is

$$\phi_{i,j}^{n+1} = \phi_{i,j}^{n} - \frac{u\Delta t}{\Delta x}(\phi_{i+1/2,j}^{n+1} - \phi_{i-1/2,j}^{n+1}) - \frac{v\Delta t}{\Delta y}(\phi_{i,j+1/2}^{n+1} - \phi_{i,j-1/2}^{n+1}) \tag{2.35}$$

where

$$\begin{aligned} \phi_{i+1/2,j} &= \phi_{i,j} + \frac{1}{2}\Psi(r_{i+1/2,j})(\phi_{i,j} - \phi_{i-1,j}) \\ \phi_{i,j+1/2} &= \phi_{i,j} + \frac{1}{2}\Psi(r_{i,j+1/2})(\phi_{i,j} - \phi_{i,j-1}) \end{aligned} \tag{2.36}$$

and

$$r_{i+1/2,j} = \frac{\phi_{i+1,j} - \phi_{i,j}}{\phi_{i,j} - \phi_{i-1,j}}, \quad r_{i,j+1/2} = \frac{\phi_{i,j+1} - \phi_{i,j}}{\phi_{i,j} - \phi_{i,j-1}} \tag{2.37}$$

The fluxes $\phi_{i-1/2,j}$ and $\phi_{i,j-1/2}$ are obtained from $\phi_{i+1/2,j}$ and $\phi_{i,j+1/2}$, respectively, by decreasing the indices by 1 in appropriate manner. If the limiter $\Psi(r)$ satisfies the conditions given in (2.27) then scheme (2.35) is monotone. This is a direct consequence of Theorem 2.1 and Definition 2.1. If the limiter Ψ satisfies (2.21) and (2.22) uniform second order accuracy is obtained.

2.2 Normalized variable technique

In [6] the SMART scheme is developed, shortly followed by the SHARP scheme [14]. Both schemes are bounded, which means that the solutions cannot contain any wiggles and remain bounded with respect to the boundary values in the absence of a physical source term. The derivation of these schemes is based on the variable normalization proposed by Leonard [14]. In the normalized variable (NV) space linear and nonlinear schemes can be constructed rather easily and the conditions for a scheme to be bounded can be clearly identified. This technique is widely used for steady-state calculations of incompressible flows (see e.g. [37], [38] and [20]). We shall give a brief description of its essential features.

For simplicity we focus on the one-dimensional situation. The multidimensional extension is straightforward. We consider the control volume surrounding point i as shown in Figure 2.1 and assume that $u_{i+1/2} > 0$. A normalized variable $\hat{\phi}$ at point $i + k$ is defined as

$$\hat{\phi}_{i+k} = \frac{\phi_{i+k} - \phi_{i-1}}{\phi_{i+1} - \phi_{i-1}}, \qquad k = -1, -\frac{1}{2}, 0, \frac{1}{2}, 1 \tag{2.38}$$

Thus, we have $\hat{\phi}_{i-1} = 0$ and $\hat{\phi}_{i+1} = 1$. The underlying principle of this variable normalization is that values of $\hat{\phi}_{i+k}$ between 0 and 1 indicate that ϕ_{i+k} is locally monotone, whereas values outside this range imply an extremum. With definition (2.38) the κ-scheme (2.3) may be written as

$$\hat{\phi}_{i+1/2} = (1 - \frac{1}{2}\kappa)\hat{\phi}_i + \frac{1}{4}(1 + \kappa) \tag{2.39}$$

whereas the first order upwind scheme, in terms of normalized variables, is simply:

$$\hat{\phi}_{i+1/2} = \hat{\phi}_i \tag{2.40}$$

Both schemes depend linearly on $\hat{\phi}_i$ only. This dependence is shown in Figure 2.3, which is called an NV diagram. The curves shown are called NV characteristics. A class of nonlinear

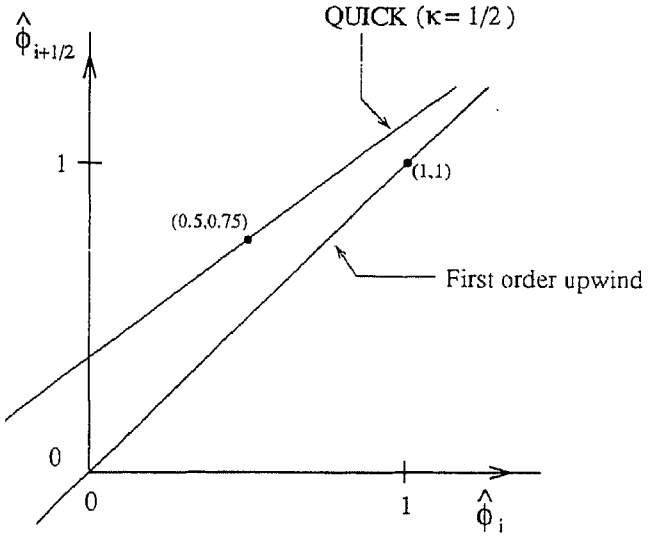

Figure 2.3: NV diagram with two well-known characteristics.

schemes is given by

$$\hat{\phi}_{i+1/2} = f(\hat{\phi}_i) \tag{2.41}$$

For such schemes the following two properties hold:

1. A scheme with a NV characteristic that passes through the point $(\frac{1}{2}, \frac{3}{4})$ in the NV diagram has second order local truncation error.

2. A scheme with a NV characteristic that satisfies $f(\frac{1}{2}) = \frac{3}{4}$ and $f'(\frac{1}{2}) = 1 - \frac{1}{2}\kappa$ has the same formal order of accuracy as the corresponding κ-scheme.

For a proof, see Appendix A. Note that all κ-schemes pass through $(\frac{1}{2}, \frac{3}{4})$.

For the construction of a bounded scheme, Gaskell and Lau [6] formulated their convection boundedness criterion (CBC) which states that if the local solution is monotone (i.e. $\phi_{i-1} \leq \phi_i \leq \phi_{i+1}$) the estimated face value $\phi_{i+1/2}$ should be between ϕ_i and ϕ_{i+1}, whereas if there is an extremum the first order upwind value must be used, i.e. $\phi_{i+1/2} = \phi_i$. The CBC implies that for $0 \leq \hat{\phi}_i \leq 1$ the NV characteristic should lie in the shaded domain of Figure 2.4 and coincide with the first order upwind NV characteristic otherwise.

The ratio of differences $\hat{\phi}_i$ (2.38) is related to the ratio of consecutive gradients $r_{i+1/2}$ (2.13) by

$$r_{i+1/2} = \frac{1 - \hat{\phi}_i}{\hat{\phi}_i} \tag{2.42}$$

This relationship allows us to convert NV schemes to flux-limited schemes and vice versa. It may be noted that based on this relationship, the SOUCUP scheme of [38] is identical to the Minmod limiter. Moreover, with the formula (2.42) it is possible to compare the CBC with

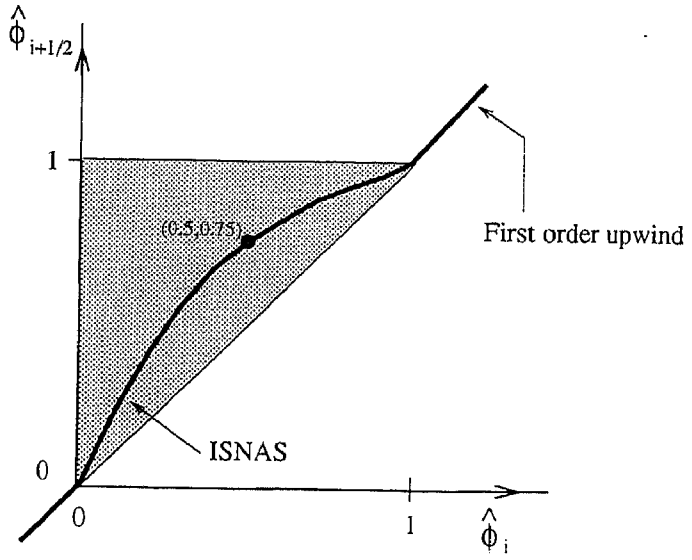

Figure 2.4: NV characteristic of ISNAS within the CBC region.

the monotonicity criterion (2.27), which is shown in Figure 2.5. Clearly, by taking $\alpha = 0$ the CBC is identical to (2.19), so that CBC implies TVD.

As an example we present a generalization of the ISNAS (Interpolation Scheme which is Nonoscillatory for Advected Scalars) flux-limited scheme proposed in [39]. In ISNAS a third order polynomial for $f(\hat{\phi}_i)$ is taken with $f(0) = 0$, $f(\frac{1}{2}) = \frac{3}{4}$, $f(1) = 1$, $f'(\frac{1}{2}) = \frac{3}{4}$ (corresponding to $\kappa = \frac{1}{2}$). See Figure 2.4. We extend this to general κ by requiring $f'(\frac{1}{2}) = 1 - \frac{1}{2}\kappa$. The following piecewise polynomials satisfy, for $\kappa \in [-1, 1]$, the CBC:

$$f(\hat{\phi}_i) = \begin{cases} \hat{\phi}_i, & \hat{\phi}_i < 0 \\ -(1+\kappa)\hat{\phi}_i^2 + (2+\frac{1}{2}\kappa)\hat{\phi}_i, & 0 \le \hat{\phi}_i \le \frac{1}{2},\ -1 \le \kappa < 0 \\ 2(\kappa+2)\hat{\phi}_i^3 - 3(\kappa+3)\hat{\phi}_i^2 + (7+\kappa)\hat{\phi}_i - 1, & \frac{1}{2} \le \hat{\phi}_i \le 1,\ -1 \le \kappa < 0 \\ 2\kappa\hat{\phi}_i^3 - (1+3\kappa)\hat{\phi}_i^2 + (2+\kappa)\hat{\phi}_i, & 0 \le \hat{\phi}_i \le 1,\ 0 \le \kappa \le 1 \\ \hat{\phi}_i, & \hat{\phi}_i > 1 \end{cases} \tag{2.43}$$

This NV formulation is easily converted to flux-limited form using (2.42). Equation (2.14) can be written as

$$\hat{\phi}_{i+1/2} = (1 + \frac{1}{2}\Psi(r_{i+1/2}))\hat{\phi}_i \tag{2.44}$$

From (2.43), (2.44) and (2.42), we deduce the following class of flux limiters:

$$\Psi_\kappa(r) = \begin{cases} (r + |r|)\,(-r^2 + (3+\kappa)r - \kappa)/(1+r)^2, & r \le 1,\ -1 \le \kappa < 0 \\ ((2+\kappa)r - \kappa)/(1+r), & r > 1,\ -1 \le \kappa < 0 \\ (r + |r|)\,((1+\kappa)r + 1 - \kappa)/(1+r)^2, & 0 \le \kappa \le 1 \end{cases} \tag{2.45}$$

which will be referred to as a rational κ (R-κ) limiter. We note that $\Psi_\kappa(1) = 1$ for all $\kappa \in [-1, 1]$. The value $\Psi'_\kappa(1) = \frac{1}{2}(1+\kappa)$ controls the accuracy, which is the same as for the

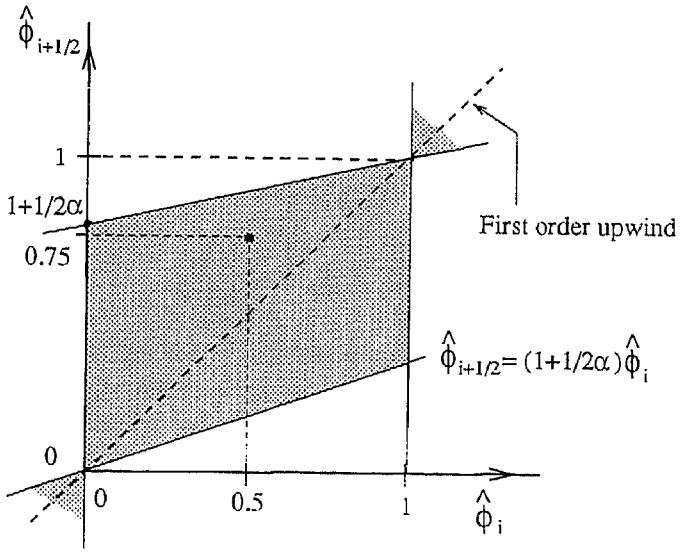

Figure 2.5: NV diagram showing the TVD region for implicit schemes.

corresponding κ-scheme. Graphical representation of the R-κ limiter for different values of κ in a flux limiter diagram is given in Figure 2.6. As expected, this figure shows that (2.19) is

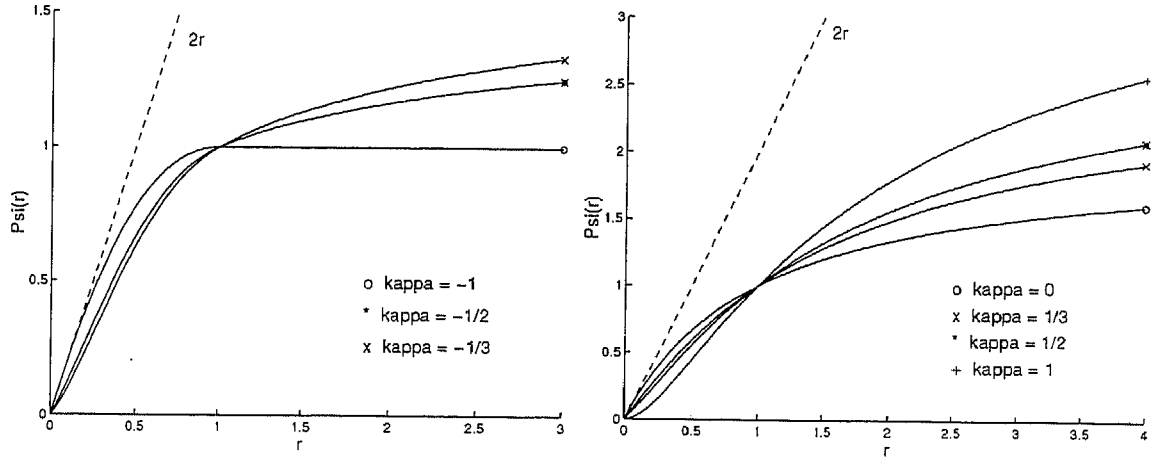

Figure 2.6: The R-κ limiter.

satisfied. For $\kappa = 0$ in (2.45) the resulting scheme is identical to the Van Leer limiter (2.20) and to the NV scheme HLPA developed in [37].

2.3 General approximation of steady-state convection: flux-limiting and defect correction strategies

We now construct a general algorithm for the approximation of cell-face fluxes in (2.2) with the different schemes previously considered by employing the flux-limiting strategy and a defect correction approach. These schemes satisfy (2.27) and are therefore monotone according to Definition 2.1, and are suitable for approximating steady-state convection according to Theorem 2.3.

The face values $\phi_{i+1/2}$ are approximated by the first order upwind scheme, corrected by

adding an appropriate anti-diffusive flux controlled by a limiter. That is, $\phi_{i+1/2}$ is approximated by

$$\phi_{i+1/2} = \begin{cases} \phi_i + \frac{1}{2}\Psi(r^+_{i+1/2})(\phi_i - \phi_{i-1}), & u_{i+1/2} > 0 \\ \phi_{i+1} - \frac{1}{2}\Psi(r^-_{i+1/2})(\phi_{i+2} - \phi_{i+1}), & u_{i+1/2} < 0 \end{cases} \tag{2.46}$$

where

$$r^+_{i+1/2} = \frac{\phi_{i+1} - \phi_i}{\phi_i - \phi_{i-1}} \quad \text{and} \quad r^-_{i+1/2} = \frac{\phi_{i+1} - \phi_i}{\phi_{i+2} - \phi_{i+1}} \tag{2.47}$$

Formula (2.46) also opens the possibility to incorporate arbitrary upwind biased schemes in an algorithmically simple way. The κ-scheme (2.3) can be written as (2.14) by taking

$$\Psi^*_\kappa(r) = \frac{1}{2}(1+\kappa)r + \frac{1}{2}(1-\kappa) \tag{2.48}$$

where the symbol $*$ indicates that this is not truly a limiter, because it does not satisfy (2.27).

This section presents five classes of flux limiters, which bring together most limiters known in the literature. The limiters presented are restricted to $\Psi(r) \geq 0$, $r \geq 0$ and degenerate locally to first order accuracy at physical extrema. If uniform second order accuracy is required, one can proceed as follows. Let a uniformly second order limiter to be constructed and a given limiter be denoted by $\tilde{\Psi}$ and Ψ^+, respectively. We assume that Ψ^+ satisfies (2.19) and (2.21). First, we compute $\Psi^+(\frac{1}{3})$, and take

$$\zeta \equiv \tilde{\Psi}(-1) = 3\Psi^+(\frac{1}{3}) - 2 \tag{2.49}$$

for uniform second order accuracy. Note that $-2 \leq \zeta \leq 0$. Next, we construct the limiter for $r < 0$, as follows:

$$\Psi^-(r) = \min[0, \max(\alpha, -\zeta r)], \quad -2 \leq \alpha \leq \zeta < 0 \tag{2.50}$$

Then, the uniformly second order limiter reads:

$$\tilde{\Psi}(r) = \frac{1}{2}[1 + \text{sign}(r)]\Psi^+(r) + \frac{1}{2}[1 - \text{sign}(r)]\Psi^-(r) \tag{2.51}$$

It is easily seen that (2.21) and (2.22) are satisfied, and condition (2.27) is satisfied, if

$$0 \leq \Psi^+ \leq (2+\alpha)r, \quad -1 \leq \alpha < 0 \tag{2.52}$$

The lower bound of α is chosen to be -1, because of the second order accuracy ($\Psi^+(1) = 1$). Together with (2.49) this leads to $-2 \leq \zeta \leq \alpha$. From (2.50) it follows that

$$\Psi^-(r) = \min[0, \max(\zeta, -\zeta r)], \quad -1 \leq \zeta < 0 \tag{2.53}$$

Finally, we require that the face value must be bounded by the neighbouring nodal values, so that

$$\frac{d\Psi^+}{dr}|_{r=0} \leq 2 + \alpha = 2 + \zeta = 3\Psi^+(\frac{1}{3}) \tag{2.54}$$

In summary, if a limiter Ψ^+ satisfies

$$\frac{1}{3} \leq \Psi^+(\frac{1}{3}) < \frac{2}{3}, \quad \frac{1}{3}\frac{d\Psi^+}{dr}(0) \leq \Psi^+(\frac{1}{3}) \tag{2.55}$$

then a uniformly second order accurate limiter can be constructed using (2.49), (2.53) and (2.51), which will fulfill (2.27). An illustration of the improvement of accuracy in this manner will be discussed in Section 4.

We shall now discuss the behaviour of several classes of flux limiters in the first quadrant of the (r, Ψ)-plane. For implicit calculations the following TVD criterion will be used:

$$0 \leq \Psi(r) \leq \min(2r, M) \tag{2.56}$$

where $M > 0$ is a parameter. This ensures that the graph of Ψ is inside the shaded region of Figure 2.2 with $\alpha = 0$. Furthermore, in the multidimensional case Definition 2.1 is satisfied, so that Theorem 2.3 applies. We are free to choose any M for obtaining bounded schemes and by increasing M more accuracy near extrema will be obtained. For $M = \infty$, condition (2.56) corresponds to CBC. Hence, any limiter previously mentioned, except Van Albada and OSPRE, can be employed.

The κ-scheme (2.48) can be made TVD by imposing constraint (2.56), resulting in the following class of flux limiters:

$$\Psi_{\kappa,\mathrm{M}}(r) = \max[0, \min(M, \frac{1}{2}(1+\kappa)r + \frac{1}{2}(1-\kappa), 2r)] \tag{2.57}$$

This is also observed by Hundsdorfer *et al.* [9]. These are called piecewise linear κ (PL-κ) limiters. This class of limiters has the advantage of high flexibility in the sense of simply switching between some linear schemes. The main disadvantage is that the non-differentiability of Ψ may adversely affect the convergence behaviour of iterative solution methods. R-κ limiters (2.45) do not share this disadvantage. Note that the parameter M controls the resolution of sharp gradients, i.e. with a large value of M more accuracy near steep gradients can be obtained. However, too large values of M may lead to convergence problems. Therefore, we take $1 \leq M \leq 4$. For $\kappa = \frac{1}{3}$ and $M = 2$ one obtains the so-called limited $\kappa = \frac{1}{3}$-scheme proposed by Koren [11]. By taking $\kappa = 1$, $1 \leq M \leq 2$ the Chakravarthy-Osher limiter is recovered. The parameters $\kappa = -1$ and $M = 1$ give the Davis limiter used in [1] and is identical to the NV scheme BSOU developed in [20]. It is interesting to note that by converting the SMART scheme of Gaskell and Lau [6] to flux-limited form, we obtain

$$\Psi_{\frac{1}{2},4}(r) = \max[0, \min(4, \frac{3}{4}r + \frac{1}{4}, 2r)] \tag{2.58}$$

which is clearly most consistent with QUICK over a maximum possible range with (2.56) for $M = 4$. An alternative is the second order symmetric UMIST limiter proposed by Lien and Leschziner [16], given by

$$\Psi(r) = \max[0, \min(2, \frac{3}{4}r + \frac{1}{4}, \frac{1}{4}r + \frac{3}{4}, 2r)] \tag{2.59}$$

Hence, this limiter is a piecewise linear version of (2.57) with $\kappa = \frac{1}{2}$, $M = 2$, which satisfies the symmetry condition (2.16). Generally, we have

$$\Psi^{s}_{\kappa,\mathrm{M}}(r) = \max[0, \min(M, \frac{1}{2}(1+\kappa)r + \frac{1}{2}(1-\kappa), \frac{1}{2}(1-\kappa)r + \frac{1}{2}(1+\kappa), 2r)] \tag{2.60}$$

which also contains the Van Leer's MUSCL scheme [31] ($\kappa = 0$, $M = 2$).

Summarizing, we now have a flux-limited scheme written in the canonical form (2.46) which comprises a number of interesting flux limiters, viz.

$$\Psi^*_\kappa(r) = \tfrac{1}{2}(1+\kappa)r + \tfrac{1}{2}(1-\kappa) \qquad \text{Linear } \kappa\text{-scheme}$$

$$\Psi_\Phi(r) = \max[\,0,\, \min(\Phi r,\, 1),\, \min(r,\, \Phi)\,] \qquad \text{Sweby } \Phi\text{-limiter}$$

$$\Psi_\kappa(r) = \begin{cases} (r+|r|)\frac{-r^2+(3+\kappa)r-\kappa}{(1+r)^2}, & r \le 1,\ -1 \le \kappa < 0 \\ \frac{(2+\kappa)r-\kappa}{1+r}, & r > 1,\ -1 \le \kappa < 0 \\ (r+|r|)\frac{(1+\kappa)r+1-\kappa}{(1+r)^2}, & 0 \le \kappa \le 1 \end{cases} \qquad \text{R-}\kappa \text{ limiter}$$

$$\Psi_{\kappa,\mathrm{M}}(r) = \max[0,\, \min(M,\, \tfrac{1}{2}(1+\kappa)r + \tfrac{1}{2}(1-\kappa),\, 2r)] \qquad \text{PL-}\kappa \text{ limiter}$$

$$\Psi^s_{\kappa,\mathrm{M}}(r) = \max[0,\, \min(M,\, \tfrac{1}{2}(1+\kappa)r + \tfrac{1}{2}(1-\kappa),\, \tfrac{1}{2}(1-\kappa)r + \tfrac{1}{2}(1+\kappa),\, 2r)] \qquad \text{Symmetric PL-}\kappa \text{ limiter}$$

where $-1 \le \kappa \le 1$, $1 \le \Phi \le 2$ and $1 \le M \le 4$. For implementation, this formulation is very convenient. Generally, the function $\Psi(r)$ is nonlinear, and more than 2 immediate neighbouring nodal points per spatial direction may be involved in approximating the convective flux $\phi_{i+1/2}$. Difficulties for iterative solution methods can be circumvented by writing $\phi_{i+1/2}$ in terms of a lower order approximation plus a correction term. This is known as the defect correction technique and was probably first used in the present context by Khosla and Rubin [10]. More specifically, the face value $\phi_{i+1/2}$ is written as

$$\phi_{i+1/2} = \phi^{\mathrm{LOS}}_{i+1/2} + (\phi^{\mathrm{HOS}}_{i+1/2} - \phi^{\mathrm{LOS}}_{i+1/2})^o \tag{2.61}$$

where $\phi^{\mathrm{LOS}}_{i+1/2}$ stands for the approximation by a lower order scheme, for example, first order upwind, and $\phi^{\mathrm{HOS}}_{i+1/2}$ is the higher order approximation. The term in brackets is evaluated explicitly using the values from the previous time step, which is indicated by the superscript 'o'. It is typically small compared to the implicit part, so that its explicit treatment does not slow down convergence. This approach ensures diagonal dominance for the resulting algebraic equations, thus enhancing iterative rate of convergence while restoring higher order accuracy at steady-state convergence. The limited anti-diffusive parts of (2.46) may be viewed as deferred corrections to the first order upwind approximation and hence can be put into the source term. Since the stencil associated with first order upwind is maintained, existing codes can easily be modified.

3 Numerical framework

The flux-limiting technique outlined in Section 2.3 has been implemented within our Navier-Stokes flow solver, which has the following features [18, 36, 24, 19, 41, 40]:

- It is based on a coordinate invariant finite volume discretization on a staggered non-orthogonal boundary-fitted grid of the incompressible Reynolds-averaged Navier-Stokes equations employing the contravariant mass flux components as primary unknowns.
- Closure of the Reynolds-averaged equations is effected by the standard k-ε model with wall functions [12].

- A second order pressure correction scheme proposed in [29] is used to obtain a divergence-free velocity field. Linearization is carried out with the Newton method.
- Time discretization takes place with a weighted average between the forward and backward Euler methods.
- The resulting algebraic equations are solved in each time step by a preconditioned GMRES solver [23]. For preconditioners we use incomplete LU factorizations. Details may be found in [34].

In every time step first the momentum and continuity equations are solved and then each turbulence equation. For time discretization the implicit Euler scheme has been selected. The process is repeated until convergence to a steady-state solution is achieved.

4 Numerical results

In this section we investigate the performance of the following schemes: the first order upwind (UDS, $\Psi = 0$), QUICK, CUI, the Fromm's scheme, ISNAS, SMART, Van Leer, the limited $\kappa = \frac{1}{3}$-scheme (i.e. PL-$\frac{1}{3}$), UMIST and MUSCL. Three two-dimensional test problems are solved. The first two cases involve convection dominance and steep gradients of the transported scalars with non-uniform and non-smooth flow fields. In the last case the numerical method is applied to a turbulent flow in which the performance of the ISNAS scheme is illustrated. To quantify the error of the schemes, the L_∞ and L_1 norms of the difference between the exact and numerical solutions are measured:

$$\|\Delta\phi\|_\infty = \max_{1\le i\le N} |\phi_{i,\text{exact}} - \phi_{i,\text{numerical}}| \tag{4.1}$$

and

$$\|\Delta\phi\|_1 = \frac{\sum_{i=1}^{N} |\phi_{i,\text{exact}} - \phi_{i,\text{numerical}}|}{N} \tag{4.2}$$

where N is the number of the grid points. Along with these measures we also give the mass error as defined by

$$|1 - r_{\text{mass}}| = |1 - \frac{\sum_{i=1}^{N} \phi_{i,\text{numerical}}}{\sum_{i=1}^{N} \phi_{i,\text{exact}}}| \tag{4.3}$$

All calculations were performed on a HP 9000/755 workstation.

The first example, which involves both a non-uniform velocity field and inclination of streamlines to grid lines, is the convection of a scalar property in a unit square transported by an inviscid stagnation flow:

$$\frac{\partial\phi}{\partial t} + \frac{\partial u\phi}{\partial x} + \frac{\partial v\phi}{\partial y} = 0, \quad (x, y) \in [0, 1] \times [0, 1] \tag{4.4}$$

with

$$(u, v) = (x, 1 - y) \tag{4.5}$$

See Figure 4.1. Non-zero inflow values are specified only for $0 \le x \le 1$ and $y = 0$ where one of the following two profiles is imposed:

$$\text{smooth profile:} \quad \phi_{\text{in}}(x) = \mathrm{e}^{-2x} \sin^2(\pi x) \tag{4.6}$$

$$\text{square wave profile:} \quad \phi_{\text{in}}(x) = \begin{cases} 1, & 0.4 \le x \le 0.6 \\ 0, & \text{otherwise} \end{cases} \tag{4.7}$$

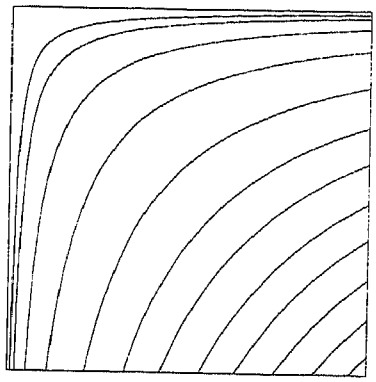

Figure 4.1: The streamlines in the stagnation flow test.

The exact solution in the first case is

$$\phi(x,y) = \mathrm{e}^{-2x(1-y)} \sin^2(\pi x(1-y)) \tag{4.8}$$

and in the second:

$$\phi(x,y) = \begin{cases} 1, & 0.4 \leq x(1-y) \leq 0.6 \\ 0, & \text{otherwise} \end{cases} \tag{4.9}$$

Three uniform grids, consisting of 30×30, 60×60 and 120×120 cells, respectively, are used. Figures 4.2 and 4.3 show the computed profiles at the outlet plane $x = 1$, obtained with these grids. The smooth solutions obtained with all schemes, except UDS, are satisfactory. For the square wave solution, QUICK, CUI and the Fromm's scheme produced results with spurious oscillations. These wiggles are effectively removed by the monotone schemes, though the UDS solution shows the worst agreement with the exact solution. Also, the higher order schemes are capable of resolving steep gradients. Furthermore, it can be seen that SMART, the limited $\kappa = \frac{1}{3}$-scheme and MUSCL yield solution slopes which are virtually the same as obtained with QUICK, CUI and the Fromm's scheme. The schemes ISNAS, Van Leer and UMIST are moderately more diffusive than the piecewise linear schemes. The error measurements are summarized in Tables 4.1 and 4.2. The maximum and mass errors for the square wave solution are not showed, because they were not thought to be meaningful. The most accurate results with respect to the smooth profile are obtained by QUICK, whereas SMART yields the smallest errors on all grids for the square wave solution. Ignoring the non-monotone schemes, the piecewise linear schemes SMART, the limited $\kappa = \frac{1}{3}$-scheme and MUSCL are more accurate than the smooth limiters ISNAS and Van Leer. The UMIST scheme gives less accurate results than its monotone rivals. In Tables 4.3 and 4.4 we give the orders of accuracy p, as measured from the medium-sized to the finest grid. For the square wave solution, we also measured the required computational cost (total CPU time, $\Delta t = 1$ s) for each scheme on the finest grid. Regarding the smooth solution, apart from UDS, all schemes show more or less second order convergence in L_1 norm. Good order behaviour is shown by MUSCL, the Fromm's scheme and the limited $\kappa = \frac{1}{3}$-scheme. The UMIST scheme and the smooth limiters ISNAS and Van Leer show a lower than $\mathcal{O}(\Delta x^2)$ behaviour with respect to $\|\Delta\phi\|_\infty$. All other schemes, except UDS, converge faster and tend to $\mathcal{O}(\Delta x^2)$. Due to the non-smoothness of the square wave solution, as expected, the order of accuracy in L_1 norm are below $\mathcal{O}(\Delta x)$. Concerning the mass errors, these are mainly caused by the fact that at the inflow boundaries the exact fluxes are imposed, whereas at the outflow boundaries - mathematically correct - the fluxes are computed from the interior numerical solution. As a

Scheme	Grid	$\|\Delta\phi\|_\infty$ $(\times 10^4)$	$\|\Delta\phi\|_1$ $(\times 10^5)$	$\|1 - r_{\text{mass}}\|$ $(\times 10^5)$
UDS	30×30	563.90	1755.00	1830.00
	60×60	316.63	928.51	933.30
	120×120	168.11	478.54	471.47
CUI	30×30	67.35	104.98	125.95
	60×60	17.04	21.09	6.61
	120×120	4.29	4.68	2.48
PL-$\frac{1}{3}$	30×30	79.30	109.69	120.28
	60×60	24.48	22.17	5.84
	120×120	5.76	4.74	2.58
QUICK	30×30	64.37	97.40	128.61
	60×60	16.33	20.36	7.61
	120×120	4.11	4.73	2.12
ISNAS	30×30	116.30	138.23	154.95
	60×60	41.28	31.59	13.21
	120×120	14.77	7.51	1.03
SMART	30×30	69.40	99.25	121.55
	60×60	20.28	20.79	6.78
	120×120	4.56	4.77	2.24
UMIST	30×30	121.00	172.86	190.47
	60×60	45.58	39.13	23.48
	120×120	17.57	9.30	1.82
Fromm	30×30	72.60	123.84	117.87
	60×60	18.40	25.20	4.27
	120×120	4.62	5.36	3.20
MUSCL	30×30	72.69	123.96	123.42
	60×60	20.98	25.81	5.20
	120×120	4.76	5.42	3.08
Van Leer	30×30	106.60	139.54	141.88
	60×60	36.28	30.01	9.21
	120×120	12.67	6.87	2.17

Table 4.1: Measured errors as function of grid spacing for the smooth case.

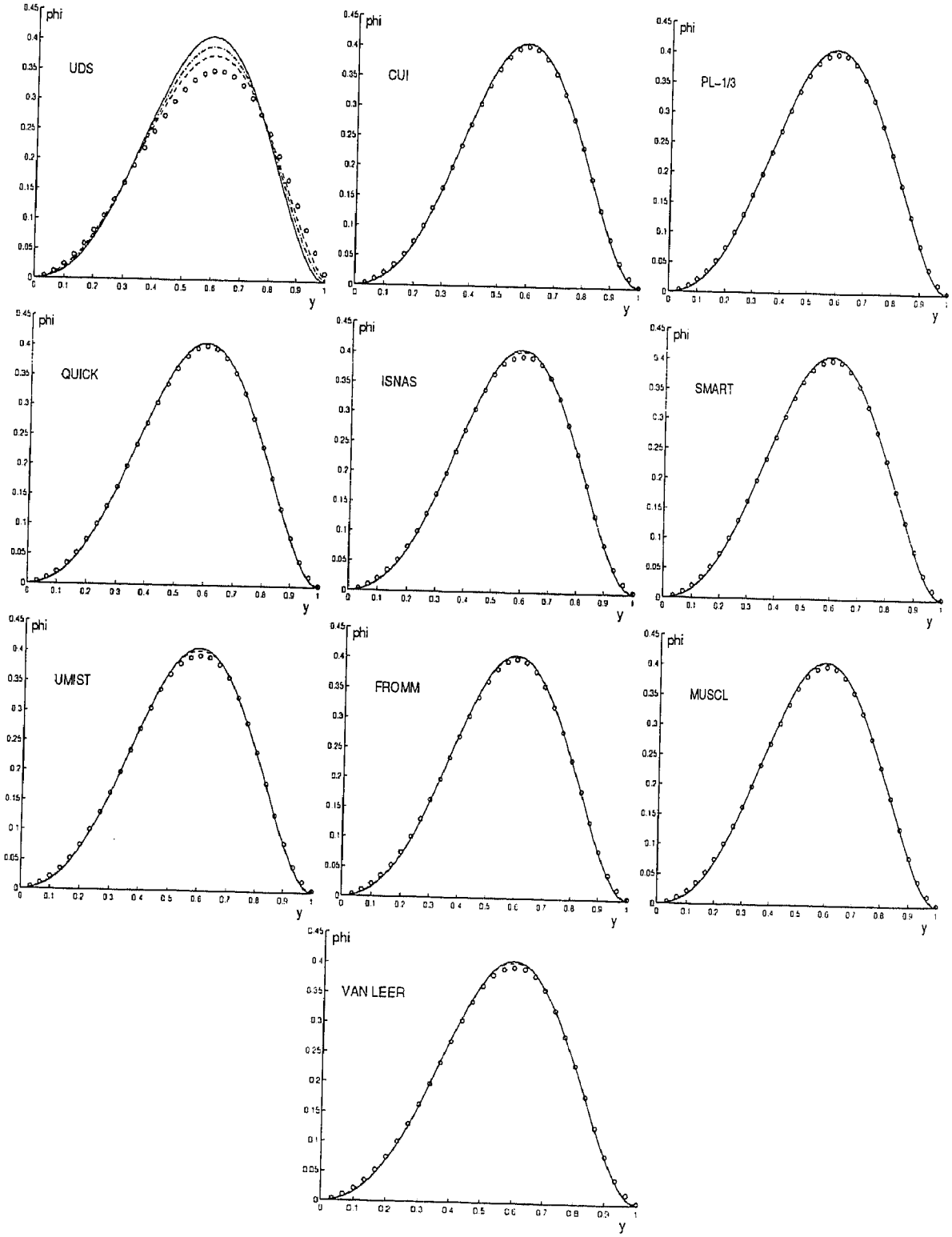

Figure 4.2: Smooth profiles at outlet. −, exact; ooo, 30 × 30; - - -, 60 × 60; -.-.-, 120 × 120.

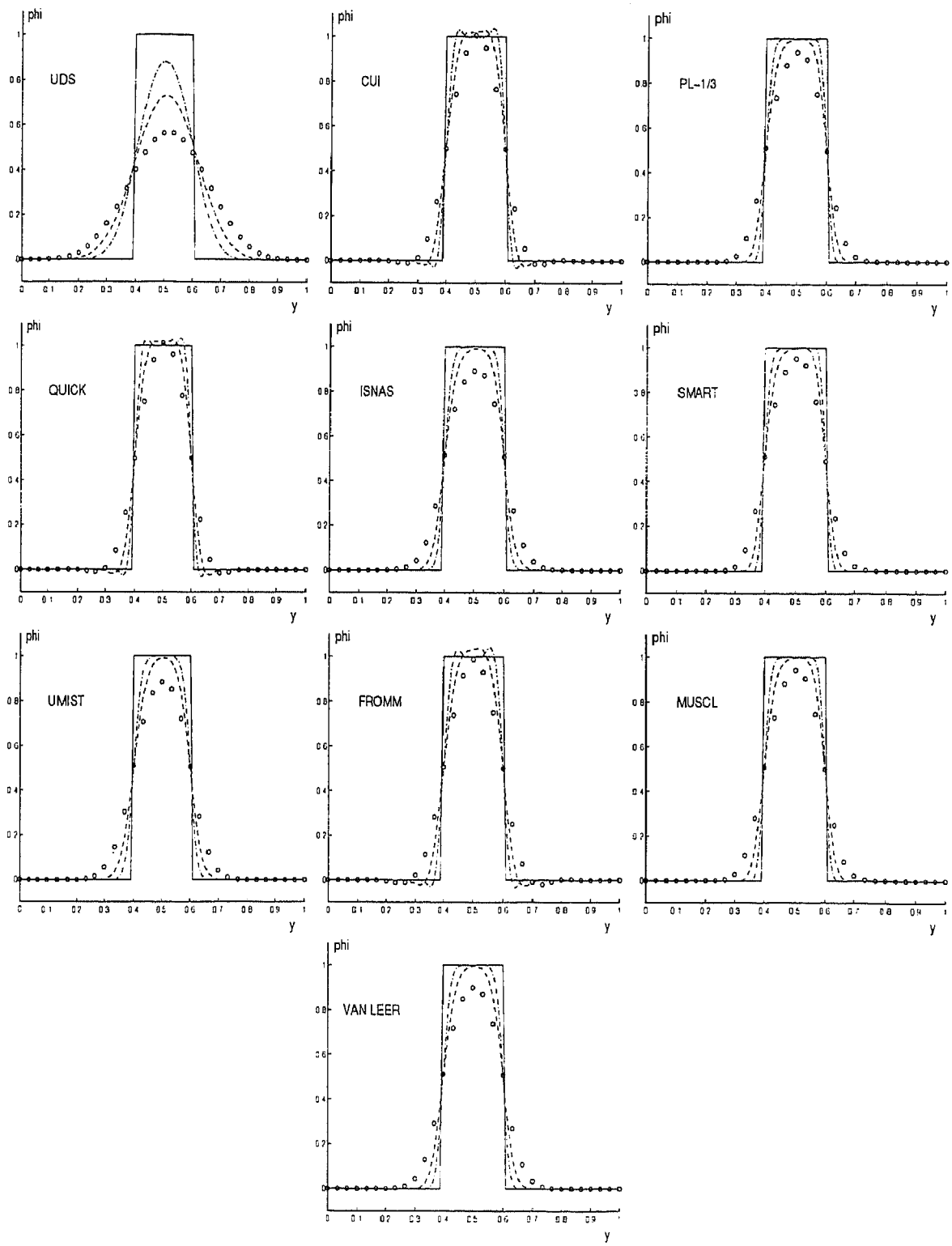

Figure 4.3: Square wave profiles at outlet. —, exact; ooo, 30×30; - - -, 60×60; -.-.-, 120×120.

Scheme	30×30	60×60	120×120
	$\|\Delta\phi\|_1$ ($\times 100$)		
UDS	9.36	6.77	4.81
CUI	4.26	2.54	1.51
PL-$\frac{1}{3}$	3.78	2.19	1.27
QUICK	4.32	2.53	1.49
ISNAS	4.12	2.46	1.47
SMART	3.55	2.04	1.18
UMIST	4.51	2.76	1.70
Fromm	4.27	2.65	1.59
MUSCL	3.89	2.26	1.32
Van Leer	4.23	2.52	1.50

Table 4.2: Measured errors as function of gridsize for the square wave case.

Scheme	$p_{\|\Delta\phi\|_\infty}$	$p_{\|\Delta\phi\|_1}$	$p_{\|1-r_{\text{mass}}\|} - p_{\|\Delta\phi\|_1}$
UDS	0.91	0.96	0.03
CUI	1.99	2.17	-0.75
PL-$\frac{1}{3}$	2.09	2.23	-1.05
QUICK	1.99	2.11	-0.27
ISNAS	1.48	2.07	1.60
SMART	2.15	2.12	-0.52
UMIST	1.38	2.07	1.62
Fromm	1.99	2.23	-1.81
MUSCL	2.14	2.25	-1.50
Van Leer	1.52	2.13	-0.04

Table 4.3: Estimated orders of several schemes for the smooth case.

Scheme	$p_{\|\Delta\phi\|_1}$	CPU (s)	# time steps
UDS	0.49	3.45	5
CUI	0.75	21.46	29
PL-$\frac{1}{3}$	0.79	94.72	128
QUICK	0.76	25.90	35
ISNAS	0.74	28.12	38
SMART	0.79	98.42	133
UMIST	0.69	14.80	20
Fromm	0.74	18.00	24
MUSCL	0.78	70.50	94
Van Leer	0.75	23.25	31

Table 4.4: Estimated order of accuracy and computing times for the square wave case.

consequence, due to discretization errors, the total net flux is not zero. Hence, schemes which are strictly conservative, do not show strictly conservation behaviour for this test case, unless - mathematically incorrect - the exact fluxes are also imposed at outflow. According to [33], a scheme has good mass conservation properties if the corresponding mass error converges better, the same, or a little bit worse than $\|\Delta\phi\|_1$. This is true for the schemes UDS, QUICK, ISNAS, SMART, UMIST and Van Leer. The remaining schemes behave not so well. Concerning the computational cost, UMIST, Van Leer and ISNAS require about 4, 7 and 8 times, respectively, more computing time than UDS and are much cheaper than SMART, the limited $\kappa = \frac{1}{3}$-scheme and MUSCL, which makes them attractive choices. This is particularly relevant for multigrid calculations.

In the next example we compare a typical TVD scheme to the uniformly second order TVD scheme to verify the improvement of accuracy of the latter. The first test case is computed again with a cone-shaped initial profile. We have selected the following flux limiters:

$$\Psi_1(r) = \max[0, \min(r, 2)], \quad \Psi_2(r) = \max[-1, \min(r, 2)] \tag{4.10}$$

The limiter Ψ_1 is the Chakravarthy-Osher or PL-1 limiter and Ψ_2 is the uniformly second order modification of Ψ_1, which satisfies (2.21) and (2.22). Note that $\kappa = 1$ is the only possibility for which the PL-κ limiter satsifies (2.55). From calculations (not shown here) it appears that the results of the smooth R-κ limiter and its modified counterpart, which satisfies (2.22), show no significant differences. Figure 4.4 shows the results of the limiters Ψ_1 and Ψ_2 compared to the exact solution, employing different grids. Clearly, the modified limiter Ψ_2 gives an improved accuracy. To quantify this improvement, the L_∞ and L_1 errors and actual orders (p) are tabulated in Table 4.5. We observe that the degeneracy to first order accuracy at maximum in the Ψ_1 limiter affects the accuracy elsewhere. The results agree with Theorem 2.2 reasonably well.

The next problem is a turbulent co-flow jet in a planar duct. The flow involves several interesting features, such as the presence of recirculation with unknown reattachment and separation points and the coexistence of both strong and weak shear regions. The geometry is a symmetric planar duct as shown in Figure 4.5. Furthermore, $d_0/D_0 = 0.075$, $U_j/U_a = 31.5$ and the Reynolds number based on D_0 and the jet flow velocity U_j is 2×10^5. Computations were performed with the standard k-ε model in conjunction with wall functions [12] on three different uniform grids, with 50×40, 70×50 and 90×60 cells. Because of symmetry, com-

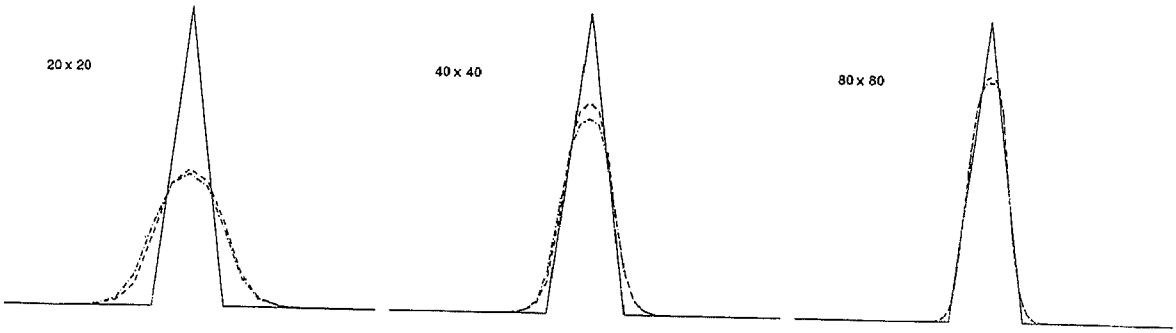

Figure 4.4: Cone profiles at outlet. —, exact; -.-.-, Ψ_1; - - -, Ψ_2.

Error	Grid	Ψ_1	p	Ψ_2	p
L_1	20×20	0.0495	-	0.0479	-
	40×40	0.0160	1.63	0.0132	1.86
	80×80	0.0051	1.65	0.0037	1.83
L_∞	20×20	0.5584	-	0.5421	-
	40×40	0.3505	0.67	0.2962	0.87
	80×80	0.2047	0.78	0.1804	0.71

Table 4.5: Errors and orders as function of grid spacing.

putations are performed in half the domain only. The convection of k and ε is approximated using the UDS and ISNAS schemes. In the momentum equations only central differences are employed. The CPU time per time step of the ISNAS scheme appears to be about 30% higher than that of UDS. Figures 4.6 and 4.7 provide a comparison of turbulent viscosity profiles arising from the UDS and ISNAS schemes, at location $x/D_0 = 1.875$. Figure 4.6 shows that in going from a coarse to a refined grid the level of turbulent viscosity calculated using the ISNAS scheme does not change much and that grid-independence has already been achieved on the 70×50 grid. As shown in Figure 4.7, the change is appreciable, however, for the first order scheme. In that case the turbulent viscosity is underestimated on both the 70×50 and 90×60 grids. Unlike UDS, ISNAS does not result in severe numerical diffusion as seen in Figures 4.6 and 4.7, where the level of turbulent viscosity obtained with UDS is lower than that of ISNAS. This can be explained as follows. In regions where the shear stress is small, the production of turbulent energy and its dissipation rate are negligible. However, the dissipation terms in the transport equations of both k and ε remain nonzero. These terms must be in balance with the transport mechanism, in particular the convective transport. Hence,

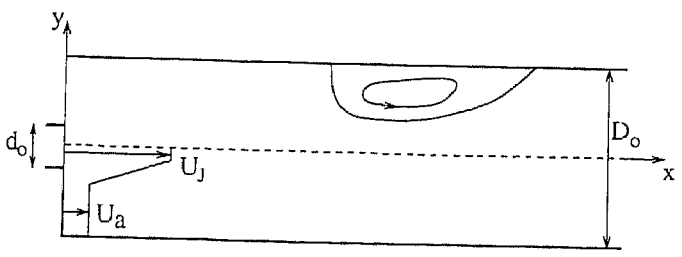

Figure 4.5: Flow configuration.

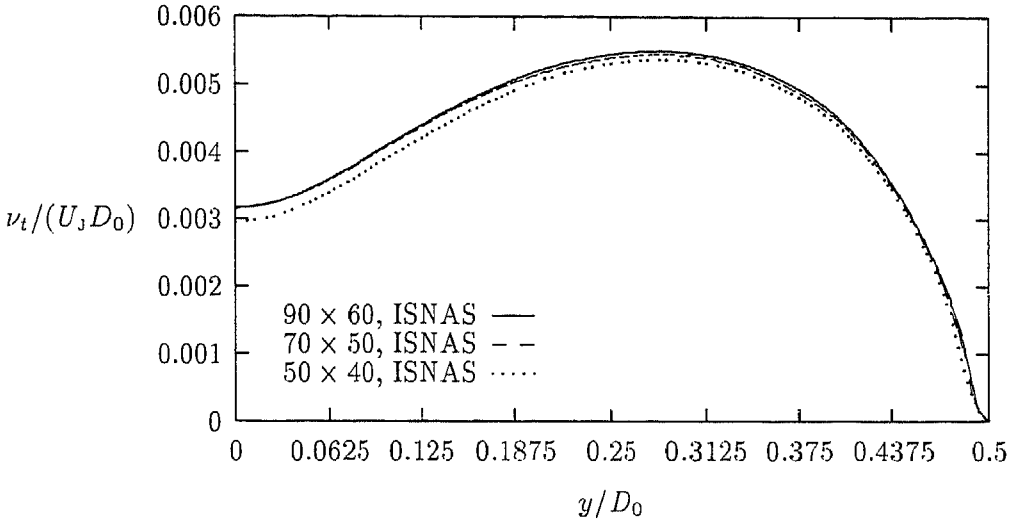

Figure 4.6: Effect of grid refinement on ν_t at $x/D_0 = 1.875$ calculated with ISNAS.

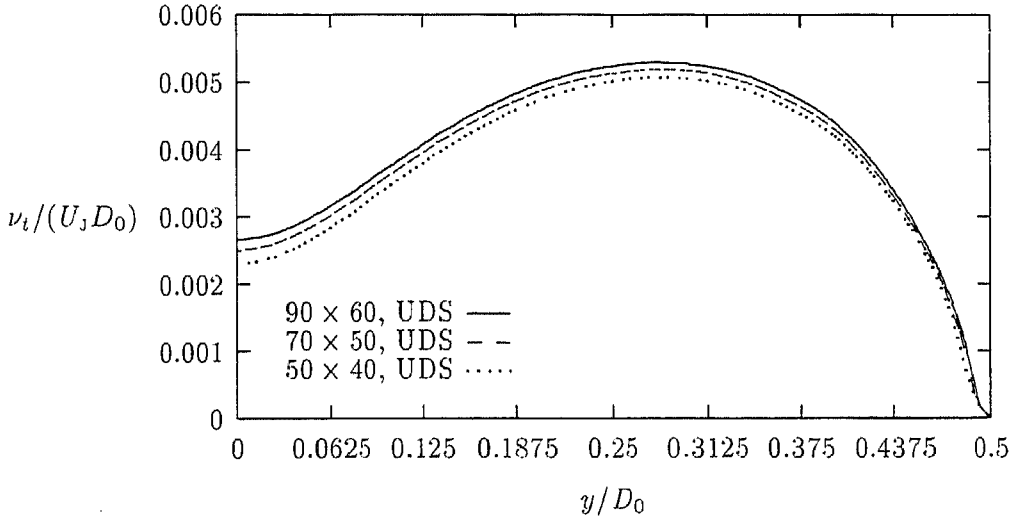

Figure 4.7: Effect of grid refinement on ν_t at $x/D_0 = 1.875$ calculated with UDS.

it is important to approximate the convection of turbulence quantities accurately. When numerical diffusion is introduced in the convection term (by UDS, for example), this leads to a too high dissipation rate ε and, since ε is a sink term in the k-equation, to too low levels of turbulent energy. As a consequence, since ν_t is proportional to k^2/ε, this double-edged effect causes ν_t to become significantly too low.

5 Conclusions

Several higher order schemes for steady-state convective transport have been presented in this paper. These have a major influence on the accuracy of turbulence models.

Based on Harten's TVD concept, sufficient conditions for an implicit scheme to be monotonicity preserving have been discussed. It has been proved that, if the flux limiters are appropriately defined, TVD schemes can be second order accurate at extrema of the solution.

contrary to what is widely believed. With Spekreijse's monotonicity concept, it is possible to carry over monotonicity properties from one dimension to two dimensions.

Two major strategies to construct nonlinear monotone schemes are flux limiting and variable normalization. These approaches have been shown to lead in similar directions, and have a one-to-one correspondence. Flux-limiting schemes can be applied easily to practical flow problems in which higher order accuracy can be maintained throughout the flow domains and the monotonicity preserving condition must be satisfied essentially.

A new class of schemes based on the κ-formulation, which preserves monotonicity, has been constructed. They are represented by second and third order polynomial interpolants in the normalized variable space satisfying CBC. These schemes have been converted to flux-limited form. This results in a class of rational κ-based limiters. For $\kappa = 0$, the Van Leer limiter is recovered, whereas a new limiter based on the QUICK scheme, called ISNAS, has been proposed.

A robust and compact algorithm using simple flux-limiting and defect correction has been outlined. This strategy encompasses a wide range of existing linear and nonlinear schemes, including those of rational and piecewise linear (symmetric and non-symmetric) κ-based formulations, and makes incorporation into general-purpose finite-volume codes feasible.

Ten schemes have been evaluated in two linear problems with pure convection, smooth and non-smooth solutions: UDS, QUICK, CUI, the Fromm's scheme, ISNAS, SMART, Van Leer, the limited $\kappa = \frac{1}{3}$-scheme, UMIST and MUSCL. The performance of each scheme have been assessed in terms of accuracy, monotonicity and efficiency. The main findings are:

- The UDS scheme suffers from excessive numerical diffusion when the flow is oblique to the grid lines and steeps gradients across the flow are present.
- The higher order schemes are substantially less numerically diffusive and accurate (for sufficiently smooth problems) than UDS; however, non-monotone schemes are prone to produce spurious oscillations, whereas monotone ones remove these wiggles effectively.
- Regarding the computational cost, the schemes ISNAS, Van Leer and UMIST are cheaper than SMART, MUSCL and the limited $\kappa = \frac{1}{3}$-scheme. However, the last three schemes give lower errors than the first three. Generally, piecewise linear limiters are less efficient than smooth ones, but very competitive in accuracy.
- The modification (4.10) of the limiter to uniform second order improves the accuracy in situations with sharp extrema.

In the computation of a confined co-flow jet in a 2D planar duct, the approximation of convection in the turbulence transport equations is shown to be of significant importance for the numerical accuracy of the solution for the k-ε turbulence model. The flux-limiting schemes are suitable for approximation of convective transport in turbulence equations, whose solutions must not, for reasons of stability, have non-physical negative values. Moreover, they can significantly reduce the grid size necessary for an accurate solution.

Acknowledgment

This investigation was supported by the Netherlands Foundation for Mathematics SMC with financial aid from the Netherlands Organization for the Advancement of Scientific Research (NWO).

A Appendix

The flux $\phi_{i+1/2}$ in (2.2) must be approximated in terms of nodal values. For example, using (2.3), we arrive at

$$\phi_{i+1/2} = a\phi_{i-1} + (\frac{1}{2} - 2a)\phi_i + (\frac{1}{2} + a)\phi_{i+1}, \quad a = -\frac{1}{4} + \frac{1}{4}\kappa \tag{A.1}$$

Let the NV characteristic be given by

$$\hat{\phi}_{i+1/2} = f(\hat{\phi}_i) \tag{A.2}$$

To find out of which linear scheme it is a nonlinear extension, f is approximated locally by

$$f(\hat{\phi}_i) = f(\alpha) + (\hat{\phi}_i - \alpha)f'(\alpha) \tag{A.3}$$

with α to be determined later. In terms of un-normalized variables, we have

$$\phi_{i+1/2} = a\phi_{i-1} + f'(\alpha)\phi_i + (f(\alpha) - \alpha f'(\alpha))\phi_{i+1} \tag{A.4}$$

We determine α and $f(\alpha)$ for (A.4) to be second order accurate. To this end, we compare with (A.1) and for second order accuracy, i.e. for all values of κ, the following must hold:

$$\frac{1}{2} + a = f(\alpha) - \alpha(\frac{1}{2} - 2a), \quad \forall a \tag{A.5}$$

or

$$\alpha = \frac{1}{2}, \quad f(\alpha) = \frac{3}{4} \tag{A.6}$$

The relation with the κ-scheme is given by

$$f'(\frac{1}{2}) = \frac{1}{2} - 2a = 1 - \frac{1}{2}\kappa \tag{A.7}$$

References

1. P. Arminjon and A. Dervieux. Construction of TVD-like artificial viscosities on two-dimensional arbitrary FEM grids. *J. Comput. Phys.*, 106:176–198, 1993.

2. D. Bradley, M. Missaghi, and S.B. Chin. A Taylor-series approach to numerical accuracy and a third-order scheme for strong convective flows. *Comput. Meth. Appl. Mech. Engng.*, 69:133–151, 1988.

3. P.J. Coelho and J.C.F. Pereira. Finite volume computation of the turbulent flow over a hill employing 2D or 3D non-orthogonal collocated grid systems. *Int. J. Numer. Meth. Fluids*, 14:423–441, 1992.

4. I. Demirdžić, A.D. Gosman, R.I. Issa, and M. Perić. A calculation procedure for turbulent flow in complex geometries. *Comput. Fluids*, 15:251–273, 1987.

5. J.E. Fromm. A method for reducing dispersion in convective difference schemes. *J. Comput. Phys.*, 3:176–189, 1968.

6. P.H. Gaskell and A.K.C. Lau. Curvature-compensated convective transport: SMART, a new boundedness-preserving transport algorithm. *Int. J. Numer. Meth. Fluids*, 8:617–641, 1988.

7. J.B. Goodman and R.J. LeVeque. On the accuracy of stable schemes for 2D scalar conservation laws. *Math. Comput.*, 45:15–21, 1985.

8. A. Harten. High resolution schemes for hyperbolic conservation laws. *J. Comput. Phys.*, 49:357–393, 1983.

9. W. Hundsdorfer, B. Koren, M. van Loon, and J.G. Verwer. A positive finite-difference advection scheme. *J. Comput. Phys.*, 117:35–46, 1995.

10. P. K. Khosla and S. G. Rubin. A diagonally dominant second-order accurate implicit scheme. *Comput. Fluids*, 2:207–209, 1974.

11. B. Koren. A robust upwind discretization method for advection, diffusion and source terms. In C.B. Vreugdenhil and B. Koren, editors, *Numerical methods for advection-diffusion problems*, pages 117–137, Vieweg, Braunschweig, Wiesbaden, 1993. Notes on Numerical Fluid Mechanics 45.

12. B.E. Launder and D.B. Spalding. The numerical computation of turbulent flows. *Comput. Meth. Appl. Mech. Engng.*, 3:269–289, 1974.

13. B.P. Leonard. A stable and accurate convective modelling procedure based on quadratic upstream interpolation. *Comput. Meth. Appl. Mech. Engng.*, 19:59–98, 1979.

14. B.P. Leonard. Simple high-accuracy resolution program for convective modelling of discontinuities. *Int. J. Numer. Meth. Fluids*, 8:1291–1318, 1988.

15. F.S. Lien and M.A. Leschziner. A general non-orthogonal collocated finite volume algorithm for turbulent flow at all speeds incorporating second-moment turbulence-transport closure, Part 1: Computational implementation and Part 2: Application. *Comput. Meth. Appl. Mech. Engng.*, 114:123–167, 1994.

16. F.S. Lien and M.A. Leschziner. Upstream monotonic interpolation for scalar transport with application to complex turbulent flows. *Int. J. Numer. Meth. Fluids*, 19:527–548, 1994.

17. M.C. Melaaen. Analysis of fluid flow in constricted tubes and ducts using body-fitted non-staggered grids. *Int. J. Numer. Meth. Fluids*, 15:895–923, 1991.

18. A.E. Mynett, P. Wesseling, A. Segal, and C.G.M. Kassels. The ISNaS incompressible Navier-Stokes solver: invariant discretization. *Appl. Sci. Res.*, 48:175–191, 1991.

19. C.W. Oosterlee, P. Wesseling, A.Segal, and E. Brakkee. Benchmark solutions for the incompressible Navier-Stokes equations in general coordinates on staggered grids. *Int J. Numer. Meth. Fluids*, 17:301–321, 1993.

20. G. Papadakis and G. Bergeles. A locally modified second order upwind scheme for convection terms discretization. *Int. J. Numer. Meth. Heat Fluid Flow*, 5:49–62, 1995.

21. S.V. Patankar. *Numerical heat transfer and fluid flow.* McGraw-Hill, New York, 1980.

22. W. Rodi, S. Majumdar, and B. Schönung. Finite volume methods for two-dimensional incompressible flows with complex boundaries. *Comput. Meth. Appl. Mech. Engng.*, 75:369–392, 1989.

23. Y. Saad and M.H. Schultz. GMRES: a generalized minimal residual algorithm for solving non symmetric linear systems. *SIAM J. Sci. Stat. Comput.*, 7:856–869, 1986.

24. A. Segal, P. Wesseling, J. van Kan, C.W. Oosterlee, and K. Kassels. Invariant discretization of the incompressible Navier-Stokes equations in boundary fitted co-ordinates. *Int. J. Numer. Meth. Fluids*, 15:411–426, 1992.

25. D.B. Spalding. A novel finite-difference formulation for differential expressions involving both first and second derivatives. *Int. J. Numer. Meth. Engng.*, 4:551–559, 1972.

26. S.P. Spekreijse. Multigrid solution of monotone second-order discretizations of hyperbolic conservation laws. *Math. Comput.*, 49:135–155, 1987.

27. S.P. Spekreijse. *Multigrid solution of the steady Euler equations.* Ph.D. thesis, Delft University of Technology, 1987.

28. P.K. Sweby. High resolution schemes using flux limiters for hyperbolic conservation laws. *SIAM J. Numer. Anal.*, 21:995–1011, 1984.

29. J.J.I.M. van Kan. A second-order accurate pressure correction method for viscous incompressible flow. *SIAM J. Sci. Stat. Comput.*, 7:870–891, 1986.

30. B. van Leer. Towards the ultimate conservative difference scheme. II. Monotonicity and conservation combined in a second order scheme. *J. Comput. Phys.*, 14:361–370, 1974.

31. B. van Leer. Towards the ultimate conservative difference scheme. V. A second-order sequel to Godunov's method. *J. Comput. Phys.*, 32:101–136, 1979.

32. B. van Leer. Upwind-difference methods for aerodynamic problems governed by the Euler equations. *Lectures in Appl. Math.*, 22:327–336, 1985.

33. C.B. Vreugdenhil and B. Koren, editors. *Numerical methods for advection-diffusion problems*, Vieweg, Braunschweig, Wiesbaden, 1993. Notes on Numerical Fluid Mechanics 45.

34. C. Vuik. Solution of the discretized incompressible Navier-Stokes equations with the GMRES method. *Int. J. Numer. Meth. Fluids*, 16:507–523, 1993.

35. N.P. Waterson and H. Deconinck. A unified approach to the design and application of bounded higher-order convection schemes. In C. Taylor and P. Durbetaki, editors, *Proc. Ninth Int. Conf. on Numer. Meth. Laminar and Turbulent Flow*, pages 203–214, Pineridge Press, Swansea, 1995.

36. P. Wesseling, A. Segal, J.J.I.M. van Kan, C.W. Oosterlee, and C.G.M. Kassels. Finite volume discretization of the incompressible Navier-Stokes equations in general coordinates on staggered grids. *Comput. Fluid Dyn. J.*, 1:27–33, 1992.

37. J. Zhu. A low-diffusive and oscillation-free convection scheme. *Comm. Appl. Numer. Meth.*, 7:225–232, 1991.

38. J. Zhu and W. Rodi. A low dispersion and bounded convection scheme. *Comput. Meth. Appl. Mech. Engng.*, 92:87–96, 1991.

39. M. Zijlema. On the construction of a third-order accurate monotone convection scheme with application to turbulent flows in general domains. *Int. J. Numer. Meth. Fluids*, 1995. To appear.

40. M. Zijlema, A. Segal, and P. Wesseling. Finite volume computation of incompressible turbulent flows in general co-ordinates on staggered grids. *Int. J. Numer. Meth. Fluids*, 20:621–640, 1995.

41. M. Zijlema, A. Segal, and P. Wesseling. Invariant discretization of the k-ε model in general co-ordinates for prediction of turbulent flow in complicated geometries. *Comput. Fluids*, 24:209–225, 1995.

The following reports have appeared in this series:

95-119	F. Périard & J.J. Kalker	Curve squeal noise by trams Part II: Wheel/rail interaction
95-120	F. Périard & J.J. Kalker	Curve squeal noise by trams Part III: Dynamic of the bogie and tram body
95-121	F. Périard & J.J. Kalker	Curve squeal noise by trams Part IV: Wheel vibration
95-122	Philippe Clément, Raúl Manásevich, Enzo Mitidieri	On a modified capillary equation
95-123	J.W. van der Woude	A graph theoretic method for computing a formal representation of the largest controlled invariant subspace of a structured system
95-124	R.J. Blok, A.E. Brouwer	Spanning point-line geometries in buildings of spherical type
95-125	Robert A. Bosch, Reinier V. Torenbeek	A family of algorithms for approximating the smallest eigenvalue of a real matrix with no complex eigenvalues
95-126	A.J. van Zanten, C. Roos and A. Snijders	A weighting system for lexicographically ordered constant-sum codes over an arbitrary alphabet
95-127	E. de Klerk, C. Roos, T. Terlaky	A nonconvex weighted potential function for polynomial target following methods
95-128	E. de Klerk, C. Roos, T. Terlaky	Semi-definite problems in truss topology optimization
95-129	W. de Jong	Simulatie van beheer als praktijkoefening
95-130	D.H.J. Epema, M. Livny, R. van Dantzig, X. Evers and J. Pruyne	A worldwide flock of Condors: load sharing among workstation clusters
95-131	M. Zijlema and P. Wesseling	Higher order flux-limiting methods for steady-state, multidimensional, convection-dominated flow

Copies of these reports may be obtained from the bureau of the Faculty of Technical Mathematics and Informatics, Julianalaan 132, 2628 BL DELFT, phone +31152784568.
A selection of these reports is available in PostScript form at the Faculty's anonymous ftp-site, ftp.twi.tudelft.nl. They are located in the directory /pub/publications/tech-reports. They can also be accessed on the World Wide Web at:
http://www.twi.tudelft.nl/TWI/Publications/Overview.html